

# Human-Like Adaptation of Force and Impedance in Stable and Unstable Interactions

Chenguang Yang, *Member, IEEE*, Gowrishankar Ganesh, *Member, IEEE*, Sami Haddadin, *Member, IEEE*, Sven Parusel, Alin Albu-Schäffer, *Member, IEEE*, and Etienne Burdet, *Member, IEEE*

**Abstract**—This paper presents a novel human-like learning controller to interact with unknown environments. Strictly derived from the minimization of instability, motion error, and effort, the controller compensates for the disturbance in the environment in interaction tasks by adapting feedforward force and impedance. In contrast with conventional learning controllers, the new controller can deal with unstable situations that are typical of tool use and gradually acquire a desired stability margin. Simulations show that this controller is a good model of human motor adaptation. Robotic implementations further demonstrate its capabilities to optimally adapt interaction with dynamic environments and humans in joint torque controlled robots and variable impedance actuators, without requiring interaction force sensing.

**Index Terms**—Feedforward force, human motor control, impedance, robotic control.

## I. INTRODUCTION

**N**EW APPLICATIONS in service robotics, health care, small-batch manufacturing, construction, entertainment, and agriculture require efficient interaction with unknown environments and human beings [1], [2]. These interactions are often unstable, e.g., when the task involves a tool or if the interaction is with an active environment. For example, carving requires compensation for the instability and unknown forces due to the contact with the raw material. While humans learn to perform

these tasks with ease, robots lack such adaptation capabilities and have generally not been conceived to deal with unstable interactions.

A robust control approach was used in most previous robotic works to guarantee interaction stability, where explicit design bounds are developed for a particular controller to maintain stability while the control structure is fixed [3]–[5]. However, human beings use a different strategy to deal with instability [6], [7]: They adapt endpoint force and viscoelasticity to compensate for the environment forces and instability by minimizing error and effort and ensuring a constant stability margin [8], [9]. Similar to humans, the learning controller that is developed in this paper increases feedforward force and impedance as long as the error is large, i.e., until the disturbing effect that results from the interaction with the environment is overcome. In the absence of a disturbance, the controller will decrease feedforward force and impedance to a small margin to keep compliance while maintaining stability.

Iterative learning control (ILC) [10], i.e., learning actuator force trial after trial along a repeated trajectory by minimizing feedback error, has produced efficient algorithms that have been demonstrated in various robotic implementations [11], and has provided an excellent model for human motor force adaptation in a novel stable interaction [12]. However, such algorithms are inefficient in unstable situations, as the force will be different in each trial due to noise or external disturbances [13]. Furthermore, safety (in particular, in a human–robot interaction) [14]–[17] and energy minimization are required to keep mechanical impedance low, which is out of the scope of ILC.

Control of the robot to match a target relation between force and displacement has been proposed in impedance control [18]. For example, an ILC approach was developed in [19] to learn the target impedance model. However, strict impedance control methods [18] require measurement of interaction forces and a fixed target impedance model so that if the environment changes drastically, the interaction may become unstable. In addition, if reproducible interaction forces are not considered, they will interfere with the impedance control.

Impedance control strategies can be optimally implemented using variable impedance actuators (VIA) [17], [20]. VIA provide robots embodied impedance as humans have through their muscles. This yields immediate response to impact as well as tunable (e.g., compliant or stiff) interaction. VIA further open possibilities of low-energy behaviors and control of viscoelasticity to improve performance in tasks such as assembly, sawing, throwing, hammering, etc., as well as for interaction with humans. However, concretizing these potentialities requires

Manuscript received December 6, 2010; revised May 4, 2011; accepted May 23, 2011. Date of publication July 5, 2011; date of current version October 6, 2011. This paper was recommended for publication by Associate Editor Y. Choi and Editor B. J. Nelson upon evaluation of the reviewers' comments. The first two authors contributed equally to the work. This work was supported in part by the European Union FP7-ICT-2007-3 VIATORS Grant.

C. Yang was with the Department of Bioengineering, Imperial College London, London, SW7 2AZ, U.K. He is now with School of Computing and Mathematics, University of Plymouth, Plymouth, PL4 8AA, U.K. (e-mail: cyang@ieee.org).

G. Ganesh was with the Department of Bioengineering, Imperial College London, London, SW7 2AZ, U.K. He is now with Computational Neuroscience Laboratories, Advanced Telecommunication Research Institute, Kyoto 6190288, Japan, and also with the National Institute of Information and Communications Technology, Japan (e-mail: gganesh@atr.jp).

S. Haddadin and S. Parusel are with the German Aerospace Center, Wessling 82234, Germany (e-mail: sami.haddadin@dlr.de; sven.parusel@dlr.de).

A. Albu-Schäffer is with the German Aerospace Center, Wessling 82234, Germany, and also with the Technical University of Munich, Munich 80333, Germany (e-mail: Alin.Albu-Schaeffer@dlr.de).

E. Burdet is with the Department of Bioengineering, Imperial College London, London, SW7 2AZ, U.K. (e-mail: eburdet@imperial.ac.uk).

This paper has supplementary downloadable material available at <http://ieeexplore.ieee.org>.

Color versions of one or more of the figures in this paper are available online at <http://ieeexplore.ieee.org>.

Digital Object Identifier 10.1109/TRO.2011.2158251

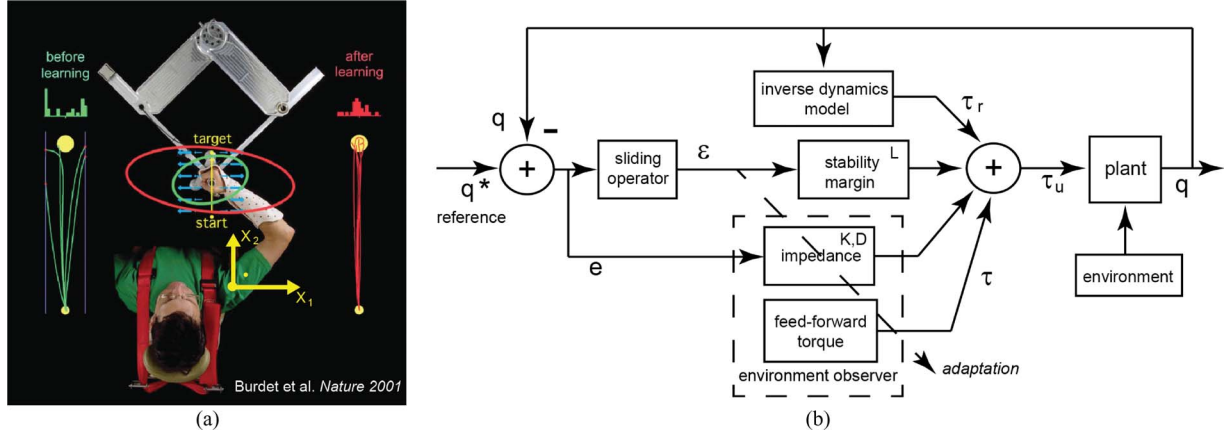


Fig. 1. Adaptation to novel dynamics: from humans to robot. (a) Investigation of point-to-point arm movements with lateral instability produced by a robotic interface showed that humans adapt mechanical impedance to ensure stable movements with minimal metabolic cost [6]. (b) Control diagram of the biomimetic controller that is presented in this paper and was derived from the results of this investigation.

appropriate algorithms to adapt force and impedance to the task and to the dynamic environment.

In this context, this paper presents an automatic motor behavior for a robot to perform tasks skillfully in unknown dynamic interactions. It starts by analyzing the control strategy that is used by the human central nervous system (CNS) in interaction tasks and then designs a biomimetic learning controller for robots using Lyapunov theory. The resulting adaptation of impedance and force is demonstrated in simulations and implemented on the 7 degree-of-freedom (DOF) DLR lightweight robot (LWR), as well as on a novel VIA [17]. The human-like adaptivity that is shown by robots in these stable and unstable tasks illustrates the potential of the novel learning controller.

## II. CONCURRENT ADAPTATION OF FORCE AND IMPEDANCE

### A. Review of Human Motor Control and Learning

To develop a controller with biomimetic adaptation properties, we first review human motor control and learning. We analyze them *from a robotics point of view* by considering the influence of both biomechanical and neural control aspects.

First, it was observed that when the human hand is slightly perturbed during arm movements, it tends to return to the undisturbed trajectory, as if the hand were connected to a spring along a planned trajectory [21]. This spring-like property stems from muscle viscoelasticity and the stretch reflex, which produce a restoring force toward the undisturbed trajectory. Analysis of this restoring force shows that the stiffness and damping increase with muscle activation [22] or endpoint force [23], and both stiffness and damping can be adapted to compensate for dynamic environments [24]. This provides *feedback* during movement due to muscle elastic property and reflexes, i.e., neural feedback.

In addition, skillful movements require a *feedforward mechanism* to plan the forces for a task in advance. Shadmehr and Mussa-Ivaldi have studied how this feedforward is acquired during performance by having subjects repeat planar arm reaching movements while interacting with a novel environment [25]. The results demonstrate that the human central nervous system

(CNS) reduces movement error trial after trial by adapting feed-forward control and compensating for the environment forces.

To manipulate objects or use tools, one has to interact with the environment and compensate for forces and instability that arise from it. While muscle intrinsic properties and reflexes generally stabilize motion, the stabilization that is provided by reflexes is limited by a time delay of at least 60 ms, which means that in some cases, reflexes can create instability [26]. Furthermore, many tasks that are common to daily life, e.g., most tasks that involve tool use, are unstable [27]. This instability will amplify the important variability that is observed in consecutive arm movements and make them unpredictable.

In a series of studies, we have analyzed the learning of stable and unstable dynamics (see Fig. 1(a), e.g., [6], [28], and [29]). We found principles of motor learning [8], [9] that yield the adaptation of both force and impedance by the concurrent minimization of motion error and effort while maintaining a fixed stability margin.

### B. Biomimetic Adaptive Controller

Let us now derive a robot controller with adaptive properties that are similar to human motor control as modeled in the previous review. In the following,  $\|\cdot\|$  denotes the Euclidean vector norm and induced matrix norm,  $\text{tr}\{\cdot\}$  stands for the trace of a matrix,  $0_{[m,n]}$  for an  $(m \times n)$ -dimensional matrix with all zero elements, and  $\otimes$  is the Kronecker product. The *task* for this controller consists of the following:

- 1) moving an  $m$  DOF robot (or a human arm) with dynamics

$$M(q)\ddot{q} + C(q, \dot{q})\dot{q} + G(q) \quad (1)$$

where  $q \in R^m$  is the joint position vector,  $M(q)$  is the (symmetric, positive definite) mass matrix,  $C(q, \dot{q})\dot{q}$  represents the torque vector due to Coriolis and centrifugal forces, and  $G(q)$  represents the torque vector due to gravity;

- 2) using actuators/muscles producing joint torques  $\tau_u$  and suffering from noise  $\tau_v(t) \leq \bar{v} < \infty$ ;

- 3) in an  $n$ -dimensional Cartesian task space ( $n \leq m$ ) that is characterized by an interaction force  $F_I(x, \dot{x}, t)$  that depends on Cartesian position  $x$ , velocity  $\dot{x}$ , and time;
- 4) while tracking a  $C^2$  bounded periodic *task reference trajectory*  $q^*(t)$ :

$$q^*(t) = q^*(t - T) < \infty, \quad T > 0. \quad (2)$$

Corresponding to the previous analysis of human motion control, we propose a robot/human controller that is composed of *feedforward and feedback* [see Fig. 1(b)], both of which are adapted during movements

$$\tau_u(t) = -\tau(t) - K(t)e(t) - D(t)\dot{e}(t) - L(t)\varepsilon(t) + \tau_r(t) \quad (3)$$

where

$$e(t) \equiv q(t) - q^*(t), \quad \dot{e}(t) \equiv \dot{q}(t) - \dot{q}^*(t)$$

are *position error* and *velocity error* relative to the task reference trajectory and

$$\varepsilon \equiv \dot{e}(t) + \kappa e(t), \quad \kappa > 0$$

is the *tracking error* commonly used in robot control [30]. In the controller (3),  $-\tau(t)$  is the *learned feedforward*, and  $-K(t)e(t) - D(t)\dot{e}(t)$  is the *feedback* due to stiffness  $K(t)$  and damping  $D(t)$  *learned through interaction with the environment*, as described in (14) and (16), shown below. The term  $-L(t)\varepsilon(t)$  corresponds to the desired *stability margin*, where  $L(t)$  is a symmetric positive-definite matrix with minimal eigenvalue

$$\lambda_{\min}(L(t)) \geq \lambda_L > 0 \quad (4)$$

that ensures stable but compliant motion control. In the human arm, this minimal feedback is produced by passive mechanical properties of muscles without contraction and reflexes [31]. To compensate for robot/arm dynamics and bounded noise, we set

$$\tau_r(t) \equiv M\ddot{q}^* + C\dot{q}^* + G - \text{sign}(\varepsilon)\bar{\nu} \quad (5)$$

with the sign function that is defined component wise.

Let  $K_E(t)$ ,  $D_E(t)$ , and  $\tau_E$  be the stiffness, damping, and feedforward torque that is required to maintain stability and to reduce systematic deviation caused by the interaction with the environment, which are represented by the vector

$$\Phi^*(t) \equiv [\text{vec}(K_E(t))^T, \text{vec}(D_E(t))^T, \tau_E^T(t)]^T \quad (6)$$

where  $\text{vec}(\cdot)$  is the column vectorization operator. Corresponding to the human motor behavior as observed in Section II-A, we assume that the CNS adapts stiffness, damping, and feedforward torque

$$\Phi(t) \equiv [\text{vec}(K(t))^T, \text{vec}(D(t))^T, \tau^T(t)]^T \quad (7)$$

such that  $\Phi(t)$  approaches the required value  $\Phi^*(t)$ , while at the same time, the CNS tends to minimize the metabolic cost so that no extra effort will be spent on the learned impedance and feedforward torque. This can be summarized as minimization of the cost function

$$V_c(t) \equiv \frac{1}{2} \int_{t-T}^t \tilde{\Phi}^T(\sigma) Q^{-1} \tilde{\Phi}(\sigma) d\sigma \quad (8)$$

where

$$\begin{aligned} \tilde{\Phi}(t) &\equiv \Phi(t) - \Phi^*(t) \\ &\equiv [\text{vec}(\tilde{K}(t))^T, \text{vec}(\tilde{D}(t))^T, \tilde{\tau}^T(t)]^T \end{aligned}$$

with

$$\begin{aligned} \tilde{K} &\equiv K(t) - K_E(t) \\ \tilde{D} &\equiv D(t) - D_E(t) \\ \tilde{\tau} &\equiv \tau(t) - \tau_E(t) \end{aligned} \quad (9)$$

and

$$Q \equiv \text{diag}(I \otimes Q_K, I \otimes Q_D, Q_\tau) \quad (10)$$

in which  $Q_K$ ,  $Q_D$ , and  $Q_\tau$  are the symmetric positive-definite matrices corresponding to the learning rate of  $K$ ,  $D$ , and  $\tau$ , respectively [see (14) and (16)]. In addition, the CNS tends to minimize motion error that is translated as concurrent minimization of

$$V_p(t) \equiv \frac{1}{2} \varepsilon^T(t) M(q) \varepsilon(t) \quad (11)$$

such that the overall cost function to minimize is

$$V(t) \equiv V_p(t) + V_c(t). \quad (12)$$

In the following, we use the motion error cost  $V_p$  of (11) as a *stability measure*. As human and robot motions have finite time, we define stability using finite time intervals. The interaction of a robot or the human body with an environment is *stable* from time  $t$ , if there is  $\delta > 0$  so that for all instant  $t_1 > t$

$$\int_t^{t_1} \dot{V}_p(\sigma) d\sigma < \delta. \quad (13)$$

Otherwise, the interaction is *unstable*. This definition, which is similar to uniformly ultimate boundedness stability [32], is illustrated by an example in Appendix A. As the evolution time is assumed to be extendable, this definition actually describes the tendency to stability/instability.

It will be shown in Section IV how this minimization of  $V(t)$  leads to the adaptation of feedforward torque and impedance as described now. Feedforward torque is adapted through

$$\begin{aligned} \delta\tau(t) &= \tau(t) - \tau(t - T) = Q_\tau (\varepsilon(t) - \gamma(t)\tau(t)) \\ \tau(t) &= 0_{[n,1]}, t \in [0, T]. \end{aligned} \quad (14)$$

where  $Q_\tau$  is a symmetric positive-definite constant matrix, and

$$\gamma(t) = \frac{a}{1 + b\|\varepsilon(t)\|^2} \quad (15)$$

is a forgetting factor of learning with positive  $a$  and  $b$ . In fact, any positive value of  $\gamma > 0$  can be used to yield the convergent result as will be shown in Section IV-A; however, a too large  $\gamma$  will prevent good buildup of torque and impedance, while a small  $\gamma$  will slow the decrease/unlearn of torque and impedance. The aforesaid definition of  $\gamma$  has the advantage that when the tracking performance is bad, i.e.,  $\varepsilon(t)$  is large, then  $\gamma(t)$  is small, and *vice versa*. The values of  $a$  and  $b$  can be selected

by the designer to adapt the response speed. The stiffness and damping matrices are adapted according to

$$\begin{aligned}\delta K(t) &= K(t) - K(t-T) \\ &= Q_K (\varepsilon(t)e^T(t) - \gamma(t)K(t)) \\ \delta D(t) &= D(t) - D(t-T) \\ &= Q_D (\varepsilon(t)\dot{e}^T(t) - \gamma(t)D(t))\end{aligned}\quad (16)$$

with  $K(t) = 0_{[n,n]}$ , and  $D(t) = 0_{[n,n]}$ ,  $t \in [0, T)$ , where  $Q_K$  and  $Q_D$  are symmetric positive-definite constant gain matrices. Section IV demonstrates that with this learning law, the controller of (3) acquires stability without using superfluous effort.

### C. Comments

1) *Force Sensing*: It is noted that the developed controller of eq. (3), together with adaptation laws (14) and (16), does not require force sensing. Therefore, no force sensor is required to implement this controller, which is an advantage as good quality force sensors are usually expensive and may not be able to detect force if the contact point is outside the measurement range.

2) *Stability Margin*: As will be illustrated by the simulation in Section III and the robotic implementation in Section V, the proposed controller can deal with both stable and unstable conditions. The learned stiffness  $K$  and damping  $D$  as well as feedforward torque  $\tau$  will compensate for the external force, such that the closed-loop dynamics of the interaction between robot and environmental force match the interaction-free behavior

$$M(q)\ddot{e} + C(q, \dot{q})\dot{e} + L\varepsilon = 0. \quad (17)$$

This is similar to the human-adaptive behavior [9], where the net impedance was observed to be maintained at the same level in various dynamic environments. In addition, as analyzed in Section IV, no extra effort will be spent to increase impedance or feedforward torque if there is no interaction or if the interaction force is assisting the tracking task.

3) *Joint Space Controller*: An interesting property of the above controller that is implemented in joint space is that the impedance is distributed according to the limbs dynamics, such that if the proximal limbs have large inertia or damping, high-frequency perturbations applied on the distal limb will lead to increase impedance mainly distally.

With the above controller, the task reference trajectory  $q^*(t)$  can be transformed from a Cartesian space reference trajectory  $x^*(t)$  by the use of a local minimization and by the integration of the transformed velocity. For example, minimization of speed  $\|\dot{q}^*\|^2$  leads to  $\dot{q}^*(t) = J^\dagger(q^*)\dot{x}^*(t)$  with the pseudo inverse  $J^\dagger \equiv J^T(JJ^T)^{-1}$  (where  $J(q)$  is the Jacobian defined through  $\dot{x} \equiv J(q)\dot{q}$ ), which can be integrated to yield the position. This transformation needs to be computed only once, e.g., offline. In addition, a desired Cartesian space impedance  $L_x(t)$  can be specified directly using the relation  $L(t) \equiv J(q^*)^T L_x(t) J(q^*)$ . Again, this transformation needs to be computed only once before starting the movement and adaptation.

4) *Cartesian Space Controller*: Equations (3)–(16) can be similarly formulated in Cartesian space. This *Cartesian space*

*controller* can be implemented (on the actuators) using

$$\tau_u \equiv J^T F_u. \quad (18)$$

If the robot position sensing is done in joint space, the Cartesian space version of the controller requires a forward kinematic transformation to compute the end effector's position in Cartesian space (in which the control force will be computed), then this force has to be transformed into joint torque and executed by the actuators. Similarly, when using VIA, embodiment of impedance requires transformation of stiffness and damping from Cartesian to joint space at every time step. These back-and-forth transformations, which must be performed at every time step, are avoided in the joint space version.

5) *Adaptive Control Extends to  $\tau_r$* : In the proposed controller, the term  $\tau_r(t)$  that is defined in (5) assumed that the model of robot/arm is exactly known such that  $M(q)$ ,  $C(q, \dot{q})$ , and  $G(q)$  are available. If the model parameters are unknown, they can be identified using adaptive control as described in Appendix B.

## III. SIMULATIONS

Before analyzing the dynamic properties of the new controller in Section IV, we first examine its efficiency and its adaptive properties through simulations. Simulations are carried on planar arm movements using the two-joint model of human arm/robot that is detailed in [13] along various movement with reference velocity profile

$$v(t) = \frac{30t^2}{T^3} \left( 1 - 2 \left( \frac{t}{T} \right) + \left( \frac{t}{T} \right)^2 \right) \frac{m}{s}. \quad (19)$$

### A. Comparison With Human Motor Control Experiments

To verify that the proposed controller is able to learn to compensate for interaction dynamics and to model human motor adaptation, we first simulate the adaptation of a point-to-point movement ahead of the body in an unstable interaction, as was tested in the experiments of [6] (see Fig. 1(a), where the right shoulder position is set as coordinate origin). We investigate the adaptation to the unstable *divergent force field* (DF)

$$F_{DF} = \begin{bmatrix} 450 & 0 \\ 0 & 0 \end{bmatrix} \begin{bmatrix} x_1 \\ x_2 \end{bmatrix} N, \quad \text{if } -0.03 \text{ m} \leq x_1 \leq 0.03 \text{ m} \\ \text{otherwise } F_{DF} = 0_{[2,2]}$$

which was used in the experiments of [6]. Note that the destabilizing force was set to zero outside of this workspace for safety reasons.

The simulation uses the reference trajectory with velocity  $v^*(t) = (x_f - x_s)v(t)$  starting at  $x_s = [0, 0.31]^T$  m and finishing at  $x_f = [0, 0.55]^T$  m, with duration  $T = 0.7$  s. The controller parameters are selected as  $Q_\tau = \text{diag}\{5, 5\}$ ,  $Q_K = \text{diag}\{80, 80\}$ ,  $Q_D = \text{diag}\{10, 10\}$ ,  $a = 0.2$ ,  $b = 5$ ,  $\kappa = 5$ , and

$$L = \begin{bmatrix} 5 & 1.2 \\ 1.2 & 4 \end{bmatrix}. \quad (20)$$

Adaptation is simulated during 60 iterations. The robust term  $\text{sign}(\varepsilon)\bar{v}$  in (5), which is specific to robot control, is not included



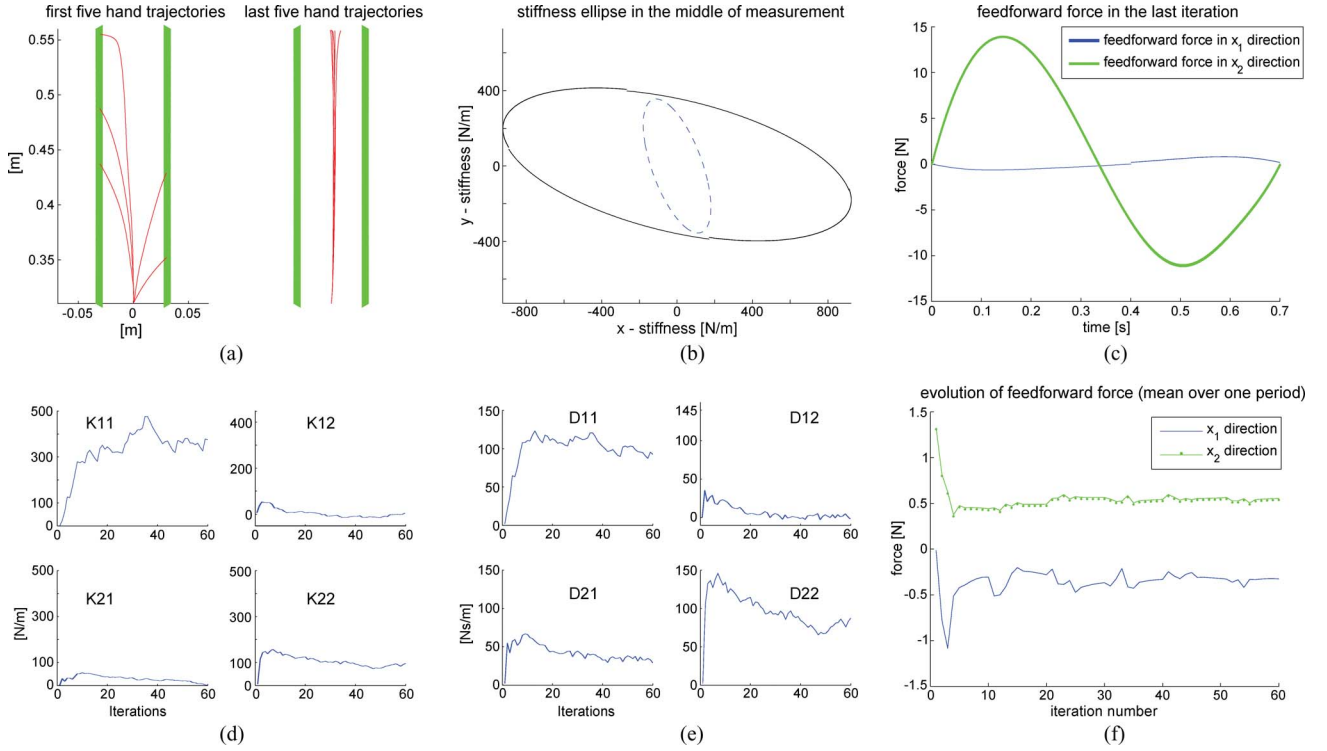


Fig. 2. Simulation of adaptation to unstable dynamics as in the experiment of [6]. (a) Hand paths before and after learning. (b) Change in the stiffness ellipse at midpoint of movement (first iteration: in dashed blue, final iteration: in solid black). (c) Feedforward force after learning in the final iteration. The evolution of (d) stiffness and (e) damping ( $2 \times 2$  matrices) and (f) force during the trials is a prediction from the model that cannot be directly compared with experiment results, as they were not measured. However, the evolution patterns are consistent with the evolution of muscle activity that is shown in [29].

in the simulation. At the end of each iteration, the position  $q$  is reset to the start point and the velocity  $\dot{q}$ , and acceleration  $\ddot{q}$  are reset to zero to emulate the experimental conditions. The noise is Gaussian with standard deviation  $\sigma = 1\text{N/m}$  truncated at  $\pm\sigma$ .

Simulation results are presented in Fig. 2. We observe similar patterns of the evolution of hand trajectories, stiffness ellipse change, and feedforward hand force after learning as in the experiments of [6]. Initial divergent trajectories become straight and successful after learning [see Fig. 2(a)]. This is caused by a selective increase in stiffness (and damping) to compensate for the unstable interaction [see Fig. 2(b), (d), and (e)] without a large modification of the feedforward force [see Fig. 2(f)].

In Fig. 2 (d)–(f), we see that stiffness and damping selectively change to maintain stability in the DF, while the feedforward force in the unstable direction (along the  $x_1$ -axis) does not vary much.

### B. Test on a Circular Tracking Task

We further test the adaptive properties of the proposed controller on the tracking of a circle of radius  $r$  centered at  $x^c$  (see the solid red line in Fig. 3) with velocity profile (19), i.e.,

$$v^*(t) = 2\pi r \begin{bmatrix} -\sin(2\pi v(t)) \\ \cos(2\pi v(t)) \end{bmatrix} \quad (21)$$

with period  $T = 1.2$  s. Three kinds of force fields are applied during motion:

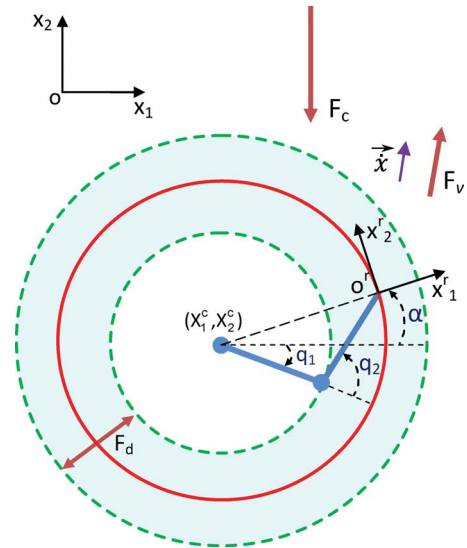


Fig. 3. Simulation of circular motion with constant force  $F_c$ , velocity-dependent divergent force  $F_v$ , and position-dependent divergent force  $F_d$ .

1) a constant interaction force field

$$F_c = \begin{bmatrix} 0 \\ -20 \end{bmatrix} \text{N}; \quad (22)$$

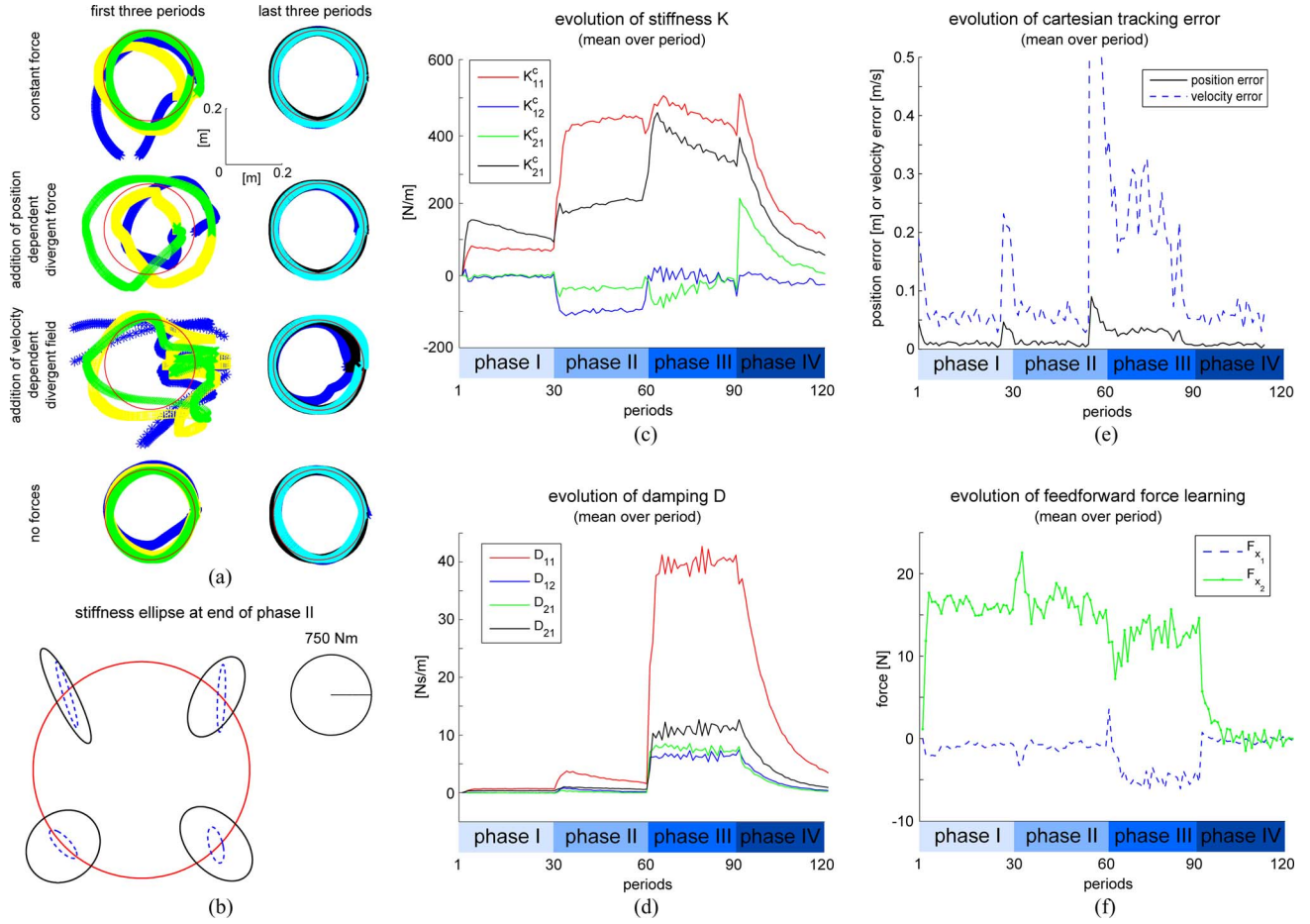


Fig. 4. Adaptation to stable and unstable position- and velocity-dependent interactions. (a) Trajectories of three consecutive periods at the beginning (1: blue; 2: yellow; 3: green) and end (1: blue; 2: black; 3: cyan) of each phase (reference trajectory in red). (b) Stiffness ellipses along the circle at the end of *phase II* with  $\kappa L$  as dashed and  $\kappa L + K$  as solid lines. (c) Evolution of the (mean over a period of) components of transformed stiffness  $K'$  in the  $x'_1 o' x'_2$  system. (d) Evolution of the (mean over a period of) components of damping  $D$  in the  $x_1 o x_2$  coordinate. (e) Average norm of errors for every periods for the three phases. (f) Evolution of feedforward force learning in the  $x_1 o x_2$  system.

2) a position-dependent DF normal to the circle

$$F_d = K_d(\|\Delta x\| - r) \frac{\Delta x}{\|\Delta x\|}, \quad \Delta x \equiv x - x^c$$

$$K_d = 450 \text{ N/m};$$

3) a velocity-dependent DF

$$F_v = K_v \dot{x}, \quad K_v = 30 \text{ Ns/m};$$

with both  $F_d$  and  $F_v$  limited to a torus within 5 cm of the circle (see the dashed green line in Fig. 3).

The task reference trajectory in joint space  $q^*(t)$  is obtained by inverse kinematics from (21). The same controller and noise parameters are used as in Section III-A.

Starting with  $K$ ,  $D$ , and  $\tau$ , all equal to zero, 120 periods of learning with the Cartesian space version of the learning controller were performed under the following conditions: *phase I*: periods 1–30 with a constant bias force  $F_I = F_c$ ; *phase II*: periods 31–60 with an additional position-dependent divergent force, i.e.,  $F_I = F_c + F_d$ ; *phase III*: periods 61–90 with additional velocity-dependent divergent force, i.e.,  $F_I =$

$F_c + F_d + F_v$ ; and *phase IV*: periods 91–120 with no interaction force.

The simulation results are presented in Fig. 4, where the stiffness ellipse, which is defined as  $\{Kx/\|x\|, x \in \mathbb{R}^2\}$ , was plotted by multiplying the Cartesian space stiffness matrix  $K \in \mathbb{R}^{2 \times 2}$  with the unit circle trajectory  $x = [\cos(\alpha), \sin(\alpha)]^T$ ,  $0 \leq \alpha < 2\pi$ . From the definition of the controller in (3), we see that initially  $K = 0_{2,2}$ , i.e., the initial stiffness is the *minimal feedback*  $\kappa L$ , while after learning the overall stiffness has been modified to  $\kappa L + K$ . Initial stiffness and overall stiffness at the end of *phase II* are plotted in Fig. 4(b) (dashed blue and solid black ellipses).

In addition, the learned stiffness  $K$  is also transformed into a moving coordinate  $x'_1 o' x'_2$  (which is shown in Fig. 3) with  $x'_1$ -axis along the radial direction and  $x'_2$ -axis normal to the radial direction. The transformed  $K'$  is calculated as  $K' = R^T(\alpha)KR(\alpha)$  with  $R(\alpha)$  the rotation matrix of angle  $\alpha$  shown in Fig. 3, and each components of  $K'$  is plotted in Fig. 4(c).

At the beginning of the simulation, when the constant force field  $F_c$  is introduced, the trajectories in consecutive periods

deviate from the circle [see the first row of Fig. 4(a)] systematically in the direction of the force. Thereafter, they monotonically converge toward the circle in less than ten periods [see *phase I* in Fig. 4(e)].

We see in the second row of Fig. 4(a) that the system becomes unstable when the position-dependent interaction force  $F_d$  is added, and the trajectory deviates in a nonsystematic way from the circle in the first trials. However after the 40th period, the system becomes able to track the circular trajectory well (see *phase II* in Fig. 4(e)). Fig. 4(b) shows that the stable behavior in *phase II* has been acquired by increasing stiffness mainly in the direction of instability, i.e., normal to the circle (along the  $x'_1$ -axis). The adaptation of the stiffness ellipse from before learning (dashed blue) to after learning (solid black) matches well with the experimental results of the human stiffness adaptation in a DF [6], [9].

When the velocity-dependent interaction force  $F_v$  is introduced, we see that the tracking performance worsens (observe the few periods starting from the 60th). However, while suitable damping  $D$  is learned [see Fig. 4(d)], the tracking improves again. The evolution of the average norm of errors [see *phase III* in Fig. 4(e)] confirms this with a large reduction in about ten periods. When all the external force fields are released at period 91, a large tracking error appears in the reverse direction due to the memory of learned feedforward force [see the last row of Fig. 4(a)]. This error, however, soon decreases to a low level [see the white part in Fig. 4(e)].

Fig. 4(c) shows the transformed stiffness  $K'$  in the  $x'_1 o' x'_2$  coordinate. We see that when the stable interaction due to  $F_c$  is introduced at period 1, stiffness changes in the very few next periods but soon tends to return back to the previous level. When the position-dependent divergent force is brought in *phase II*, the controller increases stiffness mainly in the normal direction to the circle (along  $x'_1$ ) in 30–40 periods, which reduces motion error as was just explained. Note that mainly the normal component of stiffness compensates for the interaction force, while other components are smaller.

We see in Fig. 4(f) that the feedforward force is learned at roughly the right level and during the right periods to compensate for external force  $F_c$ . Note that the level reached is slightly less than  $F_c=20$  N, probably due to the assistance that is provided by increased impedance during these periods.

### C. Comparison With Traditional Iterative Learning Control

To illustrate the difference of the novel control with respect to traditional ILC, we performed the same simulation while adapting only the feedforward force, which corresponds to ILC (but without resetting position and velocity at the beginning of every period). The results in Fig. 5 demonstrate that without impedance learning, the ILC controller is not able to perform successfully with either the divergent force  $F_d$  or the divergent force  $F_v$ , i.e., the tracking performance does not improve at all with only adaptation of feedforward force.

In contrast with the ILC method, where every iteration starts from time instant 0 to time instant  $T$ , and the values of position and velocity are reset to the fixed initial conditions ( $q_0$  and  $\dot{q}_0$ ),

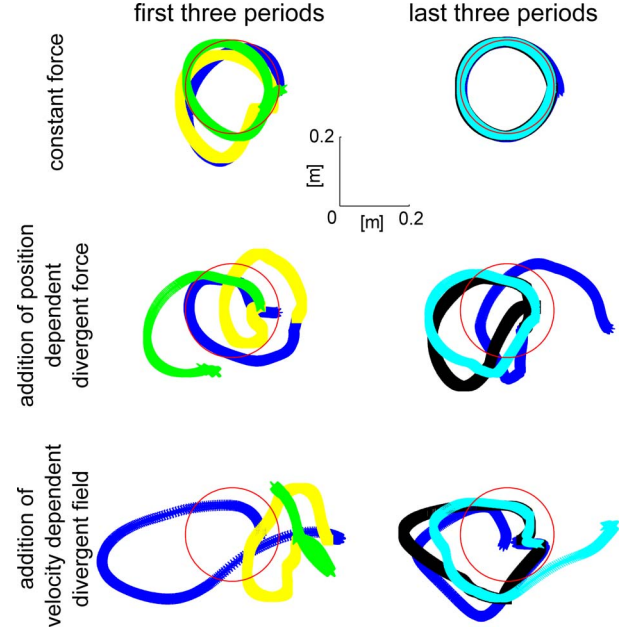


Fig. 5. Simulation result without adaptation of stiffness  $K$  and damping  $D$ .

e.g.,  $q(0) = q_0$ , and  $\dot{q}(0) = \dot{q}_0$  at each iteration, our proposed algorithm runs in a continuous manner and does not require resetting after each period.

### D. Summary

The simulation results demonstrate that the developed controller is able to acquire stability when starting with an unstable interaction. It learns to efficiently perform the tracking task with little superfluous effort, i.e., force and impedance are adapted to compensate for the environment in which the hand/robot is moving, which is similar to what was observed in the human behavior [6], [7], [28], [29]. These simulations demonstrate that the developed controller is a good model of human motor learning [9], which has promising properties as a robot controller.

## IV. STABILITY AND CONVERGENCE ANALYSIS

This section describes the convergence analysis of the joint space version of the controller. Analysis of the Cartesian space version is omitted as it is similar.

### A. Convergence Proof

The interaction force can be transformed into joint space using the forward kinematics  $x = \phi(q)$ , i.e.,

$$\tau_I(t) = J^T(q) F_I(\phi(q), J(q)\dot{q}, t) \quad (23)$$

yielding the interaction dynamics

$$M(q)\ddot{q} + C(q, \dot{q})\dot{q} + G(q) \equiv \tau_u(t) + \tau_v(t) + \tau_I(t). \quad (24)$$

For simplicity, the arguments  $q$ ,  $\dot{q}$  in  $M(q)$ ,  $C(q, \dot{q})$ , and  $G(q)$  are dropped in the following, and time index  $t$  will also be dropped sometimes in order to avoid confusion. Using the skew symmetry of the matrix  $\dot{M} - 2C$  [33], the first derivative of

$V_p(t)$  can be calculated as follows:

$$\dot{V}_p(t) = \varepsilon^T M \dot{\varepsilon} + \varepsilon^T C \varepsilon.$$

Defining

$$\dot{q}_d \equiv \dot{q}^* - \kappa e \quad (25)$$

yields [with (5)]

$$\varepsilon = \dot{q} - \dot{q}_d, \quad \dot{\varepsilon} = \ddot{q} - \ddot{q}_d. \quad (26)$$

Using (24) and (3), we obtain

$$\begin{aligned} \dot{V}_p(t) &= \varepsilon^T (\tau_\nu - \text{sign}(\varepsilon)\bar{\nu} - L\varepsilon - D\dot{\varepsilon} - Ke - \tau + \tau_I) \\ &\leq -\varepsilon^T L\varepsilon - \varepsilon^T Ke - \varepsilon^T D\dot{\varepsilon} - \varepsilon^T \tau + \varepsilon^T \tau_I \end{aligned} \quad (27)$$

from which one sees that the term  $-\text{sign}(\varepsilon)\bar{\nu}$  in (5) is used to compensate for the effect of noise  $\tau_\nu$ .

Given an interaction torque  $\tau_I$ ,  $K_E(t)$ ,  $D_E(t)$ , and  $\tau_E(t)$  represent the minimal required effort of stiffness, damping, and feedforward force (which are assumed in Section II-B) required to guarantee

$$\begin{aligned} \int_t^{t+T} \{ -\varepsilon^T(\sigma) K_E(\sigma) e(\sigma) - \varepsilon^T(\sigma) D_E(\sigma) \dot{e}(\sigma) \\ - \varepsilon^T(\sigma) \tau_E(\sigma) + \varepsilon^T(\sigma) \tau_I(\sigma) \} d\sigma \leq 0 \end{aligned} \quad (28)$$

so that from (27), we have  $\int_t^{t+T} \dot{V}_p(\sigma) d\sigma \leq 0$ . In fact, any smooth interaction force can be approximated by the linear terms of its Taylor expansion along the reference trajectory as follows:

$$\tau_I(t) = \tau_0(t) + K_I(t)e + D_I(t)\dot{e} \quad (29)$$

where  $\tau_0(t)$  is the zero-order term, and  $K_I(t)$  and  $D_I(t)$  are the first-order coefficients, which are all periodic with  $T$  (as  $q^*(t)$  in (2) is periodic). Therefore, from (29) and (26), one can obtain the values for  $K_E(t)$ ,  $D_E(t)$ , and  $\tau_E(t)$  to guarantee (28), i.e., stability. Different  $\tau_I$  will yield different values of  $K_E(t)$ ,  $D_E(t)$ , and  $\tau_E(t)$  and when  $\tau_I(t)$  is zero or is assisting the tracking task  $\|\varepsilon(t)\| \rightarrow 0$ ,  $K_E(t)$ ,  $D_E(t)$ , and  $\tau_E(t)$  will be 0.

Considering the first difference of overall cost function  $V(t)$  in (12)

$$\delta V(t) = V(t) - V(t-T) = \delta V_p(t) + \delta V_c(t). \quad (30)$$

It is shown in Appendix C that a sufficient condition for  $\delta V(t) \leq 0$  is

$$\lambda_L b \|\varepsilon\|^4 + \lambda_L \|\varepsilon\|^2 + a \|\tilde{\Phi}\|^2 - a \|\tilde{\Phi}\| \|\Phi^*\| \geq 0 \quad (31)$$

with  $\lambda_L$  defined in (4). By LaSalle's theorem, it follows that  $\|\varepsilon\|^2$  and  $\|\tilde{\Phi}\|$  will converge to an invariant set  $\Omega_s \subseteq \Omega$  on which  $\delta V(t) = 0$ , where  $\Omega$  is the bounding set that is defined as

$\Omega \equiv$

$$\left\{ (\|\varepsilon\|^2, \|\tilde{\Phi}\|), \frac{(\lambda_L b \|\varepsilon\|^2 + \frac{1}{2b})^2 + a(\|\tilde{\Phi}\| - \|\Phi^*\|/2)^2}{\frac{\lambda_L}{4b} + \frac{a\|\Phi^*\|^2}{4\lambda_L b}} \leq 1 \right\}. \quad (32)$$

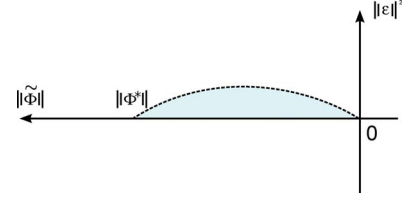


Fig. 6. Bounding set  $\Omega$  for the convergence set as defined in (32).

As illustrated in Fig. 6, the bounding set is the area in the first quadrant of an ellipse that passes through the points  $(\|\varepsilon\|^2 = 0, \|\tilde{\Phi}\| = 0)$  and  $(\|\varepsilon\|^2 = 0, \|\tilde{\Phi}\| = \|\Phi^*\|)$ . Note that if the parameter  $\gamma$  is constant, this bounding set is

$$\left\{ (\|\varepsilon\|^2, \|\tilde{\Phi}\|), \frac{4\lambda_L \|\varepsilon\|^2 + 4\gamma(\|\tilde{\Phi}\| - \|\Phi^*\|/2)^2}{\gamma \|\Phi^*\|} \leq 1 \right\}$$

i.e., as long as it is positive, the exact value of  $\gamma$  does not affect convergence; however, it will affect the speed of convergence as well as the size of convergence set.

### B. Interpretation

We see that whatever interaction disturbing the tracking task, e.g., the stable interaction force  $F_c$  and unstable interaction forces  $F_d$  and  $F_v$  in the simulation, the tracking error  $\varepsilon$  and compensation error  $\|\tilde{\Phi}\|$  will eventually fall into the (small) bounding set  $\Omega$ , which implies that the system has become stable.

In addition, since the controller aims to minimize the cost function  $V$ , which includes  $V_c$ , i.e., the measurement of the difference between learned impedance/torque and required impedance/torque to maintain stability, it will bring no extra effort in impedance/torque and thus tend to achieve optimal compensation for stable and unstable interactions.

Let us illustrate this with an example. When there is no interaction, i.e.,  $\tau_I(t) = 0$ ,  $\|\Phi^*\| = 0$ , or when the interaction force is assisting the tracking task  $\|\varepsilon\| \rightarrow 0$ , we again have  $\|\tilde{\Phi}\| = 0$  because zero values of  $K_E$ ,  $D_E$ , and  $\tau_e$  will be required. It is easy to see from Fig. 6 that  $\Omega$  shrinks to a point at origin, i.e.,  $\Omega = \{\|\varepsilon\|^2 = 0, \|\tilde{\Phi}\| = 0\}$ . It follows  $\|\tilde{\Phi}\| \rightarrow 0$ , i.e.,  $\|K\| \rightarrow 0$ ,  $\|D\| \rightarrow 0$ , and  $\|\tau\| \rightarrow 0$ , such that no effort is spent in compensation, and the control remains compliant.

In summary, the proposed control saves extra effort in the compensation of unstable interaction such that the impact with a stiff environment is minimized. When applied to VIA, the learned impedance behavior minimizes the control effort that is spent.

## V. IMPLEMENTATION AND EXPERIMENTS

The algorithm was tested on a 1-DOF DLR LWR testbed, on the DLR 7-DOF LWR arm, and on a new VIA joint. The posture control and trajectory control experiments resulted in a human-like adaptation of the feedforward torque and impedance. Videos of these experiments are attached to this paper.

Fig. 7 shows the behavior of the 1-DOF VIA joint in a *posture control experiment*. The 1-DOF system with a vertical link



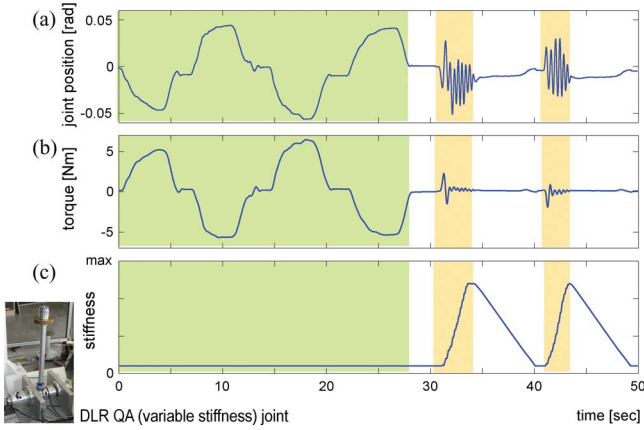


Fig. 7. Adaptation in posture control on the VIA. The robot automatically maintains its position [blue trace of (a)] in the presence of low-frequency disturbance (green region) by adapting (b) torque and reacts to high-frequency perturbations (orange) by increasing (c) stiffness.

serves as a testbed for the DLR QA joint [34]. The proposed adaptation algorithm runs on top of a low-level controller with 1-kHz rate [34]–[36] and directly commands the desired feedforward torque and impedance to it. The setup is controlled by a QNX real-time PC for low-level control that is connected to a Windows XP PC controlling the non real-time task. Parameters used in this experiment were  $Q_\tau = 9$ ,  $Q_K = 20$ ,  $Q_D = 3.0$ , and a constant  $\gamma = 0.2$ , which were selected to result in a behavior roughly similar to that observed in humans doing a similar task [37].

The robot attempts to maintain its initial position at 0 rad [see Fig. 7(a)], while a perturbation of low frequency [see the green area in Fig. 7(a)] or high frequency (orange area) is applied to the robot. The robot adapts to the vibration by changing the applied feedforward torque [see Fig. 7(b)] or impedance [see Fig. 7(c)] to minimize the deviation. When the force perturbation changes slowly, the robot applies a counter torque to reduce the deviation, with little change to impedance. However, when the perturbation frequency is higher, the robot no longer counters with torque but automatically increases its stiffness to reduce the deviation.

In the posture control experiment, the period  $T$  becomes sampling period  $\Delta t$  of the digital controller in the implementation. In the presence of a time-dependent disturbing force of low frequency ( $\ll 1/T$ ), one sees that there is a periodic time-dependent function  $\tau_0(t) = \tau_0(t - T)$  such that  $\tau_I = \tau_0$  and  $\|K_E\| = \|D_E\| = 0$  in (29). According to the convergence analysis,  $\|\hat{K}\|$  and  $\|\hat{D}\|$  will be eventually confined to a small region, thus  $K$  and  $D$  will remain small.

However, when the time-dependent disturbance is of high frequency such that  $\tau_I$  cannot be approximated only by a time-dependent periodic function  $\tau_0(t)$  (which implies that  $K_E$  and  $D_E$  cannot be zero values again), the proposed adaptation will compensate for the disturbance by increasing impedance as was seen in the experiment. Let us explain this as follows. By neglecting the small forgetting factor  $\gamma(t)$  in (14) and (16), we see that  $\|\tau(t)\|$ ,  $\|K(t)\|$ , and  $\|D(t)\|$  increase approximately linearly with the integration of  $\varepsilon = \dot{e} + \kappa e$ ,  $\text{tr}\{\varepsilon e^T\} = \frac{1}{2} \frac{d(e^T e)}{dt} + \kappa e^T e$

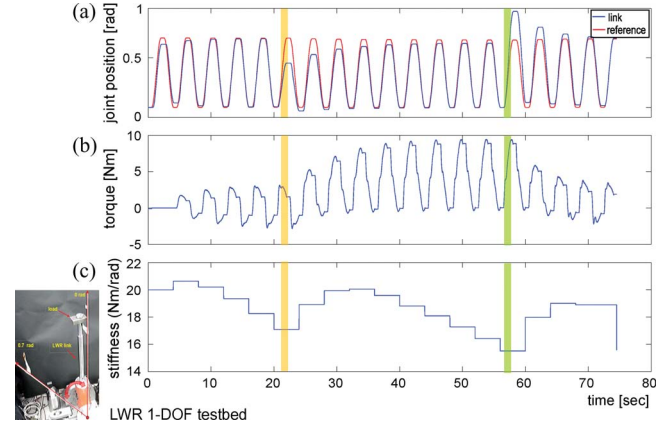


Fig. 8. Trajectory control adaptation with the 1-DOF LWR testbed. Starting with an unknown load, the periodic robot movement [(blue trace of (a))] adapts to follow the reference [red trace in (a)]. On addition (yellow) and removal (green) of a spring load, the error is compensated with trials by the change of (b) feedforward torque. (c) Impedance of the robot increases every time there are novel and, thus, unpredictable dynamics but falls once the appropriate torque profile is adapted.

and  $\text{tr}\{\varepsilon \dot{e}^T\} = \dot{e}^T \dot{e} + \frac{\kappa}{2} \frac{d(e^T e)}{dt}$ , respectively. As in the experiment, error  $e$  (as well as  $\dot{e}$ ) oscillates around zero, then  $\tau(t)$  will not change much, while  $\|K(t)\|$  and  $\|D(t)\|$  increase roughly linearly with  $\int \kappa e^T e$  and  $e^T \dot{e}$ .

A *trajectory control experiment* tested the adaptation to loads by the robot, while it had to move repetitively between 0 and 0.7 rad (see the red trace in Fig. 8). Fig. 8 plots data from implementation on the testbed of the 1-DOF LWR [38] that is controlled by a D-Space system that runs at 1 kHz with  $Q_\tau = 9$ ,  $Q_K = 95$ ,  $Q_D = 9$ , and  $\gamma = 0.5$ . The proposed adaptation algorithm runs on top of a lower level controller, which compensates for gear friction and makes the robot backdrivable [35], [36].

The experiment starts with the robot at  $0^\circ$  and with an unknown load that is fixed to the link, which causes a deviation from the reference trajectory that is reduced by adaptation in five trials. In the sixth trial, an extension spring is attached to the link, which reduces the movement amplitude [see the orange region in Fig. 8(a)]. However, the robot again learns the required torque [see Fig. 8(b)] to achieve the movement task in about nine movements. The spring is then removed in the 15th trial [see the green region in Fig. 8(a)], causing an overshoot, after which, the robot readapts to have torque levels that are similar to that of before the spring addition.

Fig. 8(b) shows the underlying torque adaptation, and Fig. 8(c) the adaptation of the stiffness of the robot during the experiment. The stiffness is initially high, but the end effector becomes more compliant as the robot adapts to the unknown load. When the spring is added, the robot increases its stiffness to quickly adapt to the induced error. However, as the robot adapts to the torque, the stiffness is reduced again. When the spring is suddenly removed, leading to an error in the task, stiffness again increases and then reduces as torque is readapted.

The 1-DOF implementations exhibited the ability of the algorithm to tune feedforward torque and impedance in magnitude. To test the ability of the adaptive control algorithm to tune

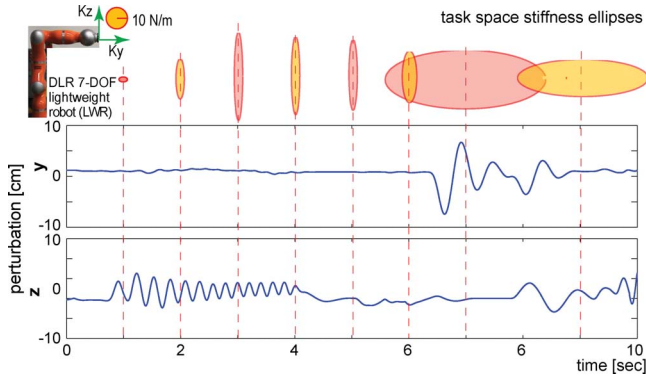


Fig. 9. Task stiffness shaping with the DLR 7-DOF LWR. The joint space implementation on the 7-DOF arm exhibits the ability of the algorithm to shape the task stiffness in magnitude and direction while maintaining a posture (which is shown in the figure) against disturbances that are applied at the end effector by a human. The 2-D projection on the  $yz$  plane of the translational task space stiffness matrix is presented at different time instances.

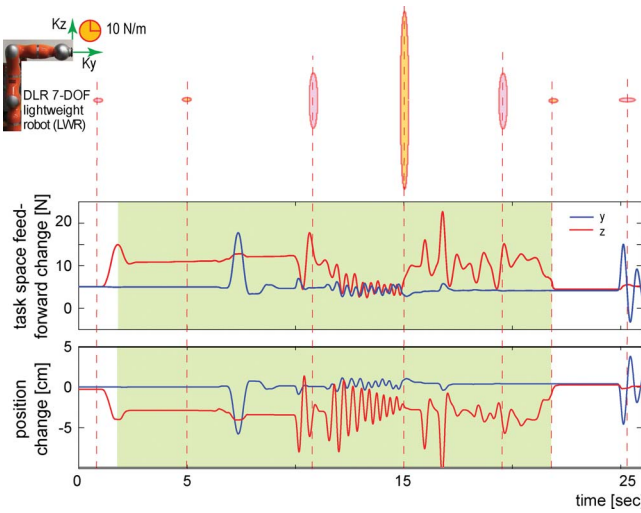


Fig. 10. Task feedforward shaping. On addition of a 0.7-kg load at the end effector (see the green region), the robot selectively increases feedforward force in the  $z$ -direction (red traces) to reduce the perturbation due to the load. There is no increase of the task space force in the  $y$ -direction.

impedance in both magnitude and geometry, a joint space implementation was performed on the 7-DOF DLR-LWR robot controlled via a VxWorks real-time system running at 1 kHz [38]. The same parameters as in the 1-DOF LWR testbed were used in each joint of the 7-DOF arm.

Fig. 9 shows the initial position of the robot, which it tries to maintain against disturbances that are generated by a human experimenter. Depending on the disturbance, the robot reacts by increasing the task space stiffness specifically in the direction of disturbance (as humans also do [6]). The disturbance may be applied on any joint or body of the robot to produce a similar result (see the attached video).

On addition of an unknown load (see the green region in Fig. 10) at the end effector, the robot learns feedforward force specifically in the  $z$ -direction without changing the force in the  $y$ -direction (see the central panel in Fig. 10). Note that the task stiffness also remains the same before (left-most ellipse) and

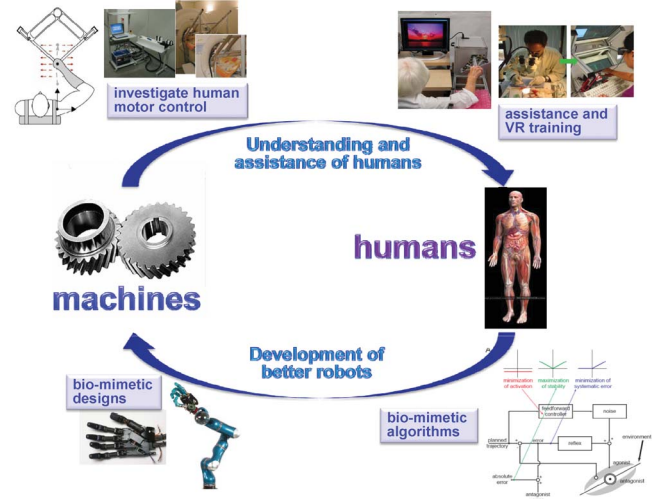


Fig. 11. Conceptual “human–machine learning cycle” showing the learning cycle between human and machine to advance understanding of human and development of better robots. On the one hand, we want to understand human motor control and provide assistive tools to humans and, on the other hand, to create better robots based on this knowledge. The control diagram in the right bottom corner is the biological version [9] of the controller that is presented in this paper.

after (second ellipse from left) the load addition, indicating that the load was compensated purely by a feedforward. The middle plot shows that impedance adaptation to a high-frequency perturbation is not modified by the new feedforward force condition.

## VI. CONCLUSION

Using robotic tools and techniques to investigate human motor control led to significant advances in our understanding of how humans control motion, as described in Section II. This in turn led to a novel robotic controller, which could simulate human motor control and learning, as shown in Section III, and was theoretically analyzed in Section IV. This novel adaptive controller, which was implemented and demonstrated, as described in Section V, can be used to assist humans (e.g., by automatically filtering tremor), or in rehabilitation robots, providing guiding assistance adapted to the patient and her or his state. This embodies one of the very first examples of the virtuous *human–machine motor learning cycle* (see Fig. 11) in which progresses in neuroscience and neurology lead to robotic advances, and conversely.

Specifically, a *novel adaptive motor behavior* has been created, which is both a successful model of human motor adaptation that is able to predict all published observations on impedance adaptation [9], as well as a robotic controller with the following properties.

- 1) It is the first controller that is able to simultaneously adapt force and impedance in the presence of unknown dynamics.
- 2) It can deal with unstable situations that are typical of tool use and gradually acquire a desired stability margin.
- 3) It does not require interaction force sensing.

- 4) It is strictly derived from the minimization of motion error and effort.
- 5) It is an intuitive adaptive solution for a human–robot interaction, such as what is needed in rehabilitation, physical training, and teleoperation.

The controller was validated in implementations with one and multi-DOF force controlled robots, can utilize the new possibilities offered by VIA, and can realize optimal assistance in a human–machine interaction.

## APPENDIX A

### STABILITY MEASURE

This Appendix illustrates the stability definition of eq. (13) through an unstable interaction example. For simplicity, we assume that there is no adaptation of stiffness, damping, or feedforward torque, i.e.,  $K$ ,  $D$ , and  $\tau$  equal zero in controller (3), and there is an interaction torque  $\tau_I = K_I e + D_I \dot{e}$  with positive-definite constant matrices  $K_I$  and  $D_I$ , from time  $t$ . For simplicity, we neglect the effect of noise and the robust term  $\text{sign}(\varepsilon)\bar{\nu}$ , and assume that at the starting time  $t$ ,  $\dot{e}(t) = e(t) = 0_{[n,1]}$ . Using (27) yields

$$\begin{aligned} \int_t^{t_1} \dot{V}_p(\sigma) d\sigma &= \int_t^{t_1} \varepsilon^T K_I e + \varepsilon^T D_I \dot{e} - \varepsilon^T L \varepsilon d\sigma \\ &= \int_t^{t_1} \kappa e^T (K_I - \kappa L) e + \dot{e}^T (D_I - L) \dot{e} d\sigma \\ &\quad + \frac{1}{2} e^T (K_I + \kappa D_I - 2\kappa L) e + \frac{\kappa}{2} e^T D_I e. \end{aligned} \quad (33)$$

Noting that [using (11) and (4)]  $V_p \leq \lambda_M (\dot{e}(t) + \kappa e(t))^T (\dot{e}(t) + \kappa e(t))$  with  $\lambda_M$  denoting the largest eigenvalue of  $M(q)$ , it can be shown from (33) that when  $K_I > \kappa L$  and  $D_I > L$ , there exists a constant scalar  $g$  such that  $\int_t^{t_1} [\dot{V}_p(\sigma) - g V_p(\sigma)] d\sigma > 0$ , and then, it can be further shown that for any  $\delta$ , there exists a time instant  $t_1$  to make  $\int_t^{t_1} \dot{V}_p(\sigma) d\sigma > \delta$  hold. This implies that the closed-loop dynamics is unstable from time  $t$ .

## APPENDIX B

### IDENTIFICATION OF THE ROBOT'S PARAMETERS

If the structure of the robot's dynamics is known but the actual robot parameters  $p \in \mathbb{R}^p$  are unknown, e.g., the rigid body dynamics model can be written as

$$\Psi(\ddot{q}^*, \dot{q}^*, \dot{q}, q) p \equiv M(q) \ddot{q}^* + C(q, \dot{q}) \dot{q}^* + G(q) \quad (34)$$

with known  $\Psi$  and unknown  $p$ , then the unknown parameters  $p$  can be identified online using the learning law [39]

$$\hat{p}(t) = \hat{p}(t-T) - S \Psi(\ddot{q}^*, \dot{q}^*, \dot{q}, q)^T \varepsilon(t) \quad (35)$$

where  $S$  is a symmetric positive-definite matrix, and  $\Psi(\ddot{q}^*, \dot{q}^*, \dot{q}, q)$  is the regressor matrix, together with the learning of feedforward (14) and impedance (16). Then, we can set

$$\tau_r(t) = \Psi(\ddot{q}^*, \dot{q}^*, \dot{q}, q) \hat{p}(t) - \text{sign}(\varepsilon) \bar{\nu} \quad (36)$$

corresponding to adding, to the cost function (12), the following term:

$$V_l(t) = \int_{t-T}^t \tilde{p}^T(\tau) S^{-1} \tilde{p}(\tau) d\tau \quad (37)$$

with the same results as in Section IV-A.

## APPENDIX C

### DERIVATION OF EQ. (31)

In the following, we show that (31) is sufficient to guarantee  $\delta V(k) > 0$ . As can be seen from (30),  $\delta V(k)$  consists of two parts:  $\delta V_p(t)$  and  $\delta V_c(t)$ . Let us first analyze  $\delta V_p(t)$ , for which the following can be derived from (9), (27), and (28)

$$\begin{aligned} \delta V_p(t) &= V_p(t) - V_p(t-T) \\ &\leq \int_{t-T}^t -\varepsilon^T(\sigma) L(\sigma) \varepsilon(\sigma) - \varepsilon^T \tilde{K}(\sigma) e(\sigma) \\ &\quad - \varepsilon^T(\sigma) \tilde{D}(\sigma) \dot{e}(\sigma) - \varepsilon^T(\sigma) \tilde{\tau}(\sigma) \\ &\quad - \varepsilon^T K_E e - \varepsilon^T D_E \dot{e} - \varepsilon^T \tau_E + \varepsilon^T \tau_I d\sigma \\ &\leq \int_{t-T}^t -\varepsilon^T(\sigma) L(\sigma) \varepsilon(\sigma) - \varepsilon^T \tilde{K}(\sigma) e(\sigma) \\ &\quad - \varepsilon^T(\sigma) \tilde{D}(\sigma) \dot{e}(\sigma) - \varepsilon^T(\sigma) \tilde{\tau}(\sigma) d\sigma. \end{aligned} \quad (38)$$

We now turn our attention to the first difference of the cost function  $\delta V_c(t) = V_c(t) - V_c(t-T)$ . According to the definition of  $\Phi(t)$  and  $Q$  in (7) and (10), we have

$$\begin{aligned} \delta V_c(t) &= \frac{1}{2} \int_{t-T}^t \{ \text{tr} \{ \tilde{K}^T(\sigma) Q_K^{-1} \tilde{K}(\sigma) - \tilde{K}^T(\sigma-T) Q_K^{-1} \tilde{K}(\sigma-T) \} \\ &\quad + \text{tr} \{ \tilde{D}^T(\sigma) Q_D^{-1} \tilde{D}(\sigma) - \tilde{D}^T(\sigma-T) Q_D^{-1} \tilde{D}(\sigma-T) \} \\ &\quad + \tilde{\tau}^T(\sigma) Q_\tau^{-1} \tilde{\tau}(\sigma) - \tilde{\tau}^T(\sigma-T) Q_\tau^{-1} \tilde{\tau}(\sigma-T) \} d\sigma. \end{aligned} \quad (39)$$

Now, we rewrite (14) and (16) as

$$\begin{aligned} \delta \tilde{K}(t) &= Q_K (\varepsilon(t) e^T(t) - \gamma(t) K(t)) \\ \delta \tilde{D}(t) &= Q_D (\varepsilon(t) \dot{e}^T(t) - \gamma(t) D(t)) \\ \delta \tilde{\tau}(t) &= Q_\tau (\varepsilon - \gamma(t) \tau(t)). \end{aligned} \quad (40)$$

Using (40), the symmetry of  $Q_K^{-1}$  and the fact  $\tilde{K}(\sigma) - \tilde{K}(\sigma-T) = \delta K(\sigma)$ , one can show that the first term in the integrand of (39) can be written as

$$\begin{aligned} &\text{tr} \{ \tilde{K}^T(\sigma) Q_K^{-1} \tilde{K}(\sigma) - \tilde{K}^T(\sigma-T) Q_K^{-1} \tilde{K}(\sigma-T) \} \\ &= \text{tr} \{ (\tilde{K}(\sigma) - \tilde{K}(\sigma-T))^T Q_K^{-1} \\ &\quad \times (2\tilde{K}(\sigma) - \tilde{K}(\sigma) + \tilde{K}(\sigma-T)) \} \\ &= \text{tr} \{ \delta K^T(\sigma) Q_K^{-1} (2\tilde{K}(\sigma) - \delta K(\sigma)) \} \\ &= -\text{tr} \{ \delta K^T(\sigma) Q_K^{-1} \delta K(\sigma) \} + 2\text{tr} \{ \delta K^T(\sigma) Q_K^{-1} \tilde{K}(\sigma) \} \\ &= -\text{tr} \{ \delta K^T(\sigma) Q_K^{-1} \delta K(\sigma) \} \\ &\quad + 2\varepsilon^T(\sigma) \tilde{K}(\sigma) e(\sigma) - 2\gamma(\sigma) \text{tr} \{ K^T(\sigma) \tilde{K}(\sigma) \}. \end{aligned} \quad (41)$$



Performing a similar derivation for the second and third terms in the integrand of (39), we have

$$\begin{aligned} & \text{tr}\{\tilde{D}^T(\sigma)Q_D^{-1}\tilde{D}(\sigma) - \tilde{D}^T(\sigma - T)Q_D^{-1}\tilde{D}(\sigma - T)\} \\ &= -\text{tr}\{\delta D^T(\sigma)Q_D^{-1}\delta D(\sigma)\} + 2\varepsilon^T(\sigma)\tilde{D}(\sigma)\dot{\varepsilon}(\sigma) \\ & \quad - 2\gamma(\sigma)\text{tr}\{D^T(\sigma)\tilde{D}(\sigma)\} \end{aligned} \quad (42)$$

and

$$\begin{aligned} & \text{tr}\{\tilde{\tau}^T(\sigma)Q_\tau^{-1}\tilde{\tau}(\sigma) - \tilde{\tau}^T(\sigma - T)Q_\tau^{-1}\tilde{\tau}(\sigma - T)\} \\ &= -\text{tr}\{\delta\tau^T(\sigma)Q_\tau^{-1}\delta\tau(\sigma)\} + 2\varepsilon^T(\sigma)\tilde{\tau}(\sigma) \\ & \quad - 2\gamma(\sigma)\text{tr}\{\tau^T(\sigma)\tilde{\tau}(\sigma)\}. \end{aligned} \quad (43)$$

Incorporating (41), (42) and (43) into (39), we finally obtain

$$\begin{aligned} \delta V_c(t) &= -\frac{1}{2} \int_{t-T}^t \delta\tilde{\Phi}^T(\sigma)Q^{-1}\delta\tilde{\Phi}(\sigma) d\sigma \\ & \quad - \int_{t-T}^t \gamma(\sigma)\tilde{\Phi}^T(\sigma)\Phi(\sigma) d\sigma \\ & \quad + \int_{t-T}^t \varepsilon^T(\sigma)\tilde{K}(\sigma)e(\sigma) + \varepsilon^T(\sigma)\tilde{D}(\sigma)\dot{\varepsilon}(\sigma) \\ & \quad + \varepsilon^T(\sigma)\tilde{\tau}(\sigma) d\sigma. \end{aligned} \quad (44)$$

Combining with (38) yields

$$\begin{aligned} \delta V(t) &= V(t) - V(t - T) = \delta V_p(t) + \delta V_c(t) \\ &\leq -\frac{1}{2} \int_{t-T}^t \delta\tilde{\Phi}^T(\sigma)Q^{-1}\delta\tilde{\Phi}(\sigma) d\sigma - \int_{t-T}^t \varepsilon^T(\sigma)L(\sigma)\varepsilon(\sigma) \\ & \quad + \gamma(\sigma)\tilde{\Phi}^T(\sigma)\tilde{\Phi}(\sigma) \\ & \quad + \gamma(\sigma)\tilde{\Phi}^T(\sigma)\Phi^*(\sigma) d\sigma. \end{aligned} \quad (45)$$

A sufficient condition to make  $\delta V(t)$  in (45) non-positive is

$$\begin{aligned} & \varepsilon^T L \varepsilon + \gamma \tilde{\Phi}^T \tilde{\Phi} + \gamma \tilde{\Phi}^T \Phi^* \\ & \geq \lambda_L \|\varepsilon\|^2 + \gamma \|\tilde{\Phi}\|^2 - \gamma \|\tilde{\Phi}\| \|\Phi^*\| \geq 0 \end{aligned} \quad (46)$$

where  $\lambda_L$  was defined in (4) as the infimum of the smallest eigenvalue of  $L$ . Substituting  $\gamma(t) = \frac{a}{1+b\|\varepsilon\|^2}$  into the above inequality yields the inequality of (31).

#### ACKNOWLEDGMENT

The authors would like to thank N. Jarrasse for editing of the figures and text.

#### REFERENCES

- [1] M. A. Peshkin and J. E. Colgate, "Cobots," *Ind. Robot: Int. J.*, vol. 26, no. 5, pp. 33–34, 1999.
- [2] O. Lambercy, L. Dovat, R. Gassert, E. Burdet, C. L. Teo, and T. Milner, "A haptic knob for rehabilitation of hand function," *IEEE Trans. Neural Syst. Rehabil. Eng.*, vol. 15, no. 3, pp. 356–366, Sep. 2007.
- [3] J. E. Colgate and N. Hogan, "Robust control of dynamically interacting systems," *Int. J. Control*, vol. 48, no. 1, pp. 65–88, 1988.
- [4] N. Hogan, "On the stability of manipulators performing contact tasks," *IEEE J. Robot. Autom.*, vol. 4, no. 6, pp. 677–686, Dec. 1988.
- [5] J. E. Colgate, "Coordinate transformations and logical operations for minimizing conservativeness in coupled stability criteria," *J. Dyn. Syst., Meas. Control*, vol. 116, no. 4, pp. 643–649, 1994.
- [6] E. Burdet, R. Osu, D. W. Franklin, T. E. Milner, and M. Kawato, "The central nervous system stabilizes unstable dynamics by learning optimal impedance," *Nature*, vol. 414, no. 6862, pp. 446–449, 2001.
- [7] D. W. Franklin, G. Liaw, T. E. Milner, R. Osu, E. Burdet, and M. Kawato, "Endpoint stiffness of the arm is directionally tuned to instability in the environment," *J. Neurosci.*, vol. 27, no. 29, pp. 7705–7716, 2007.
- [8] D. W. Franklin, E. Burdet, K. P. Tee, R. Osu, C. M. Chew, T. E. Milner, and M. Kawato, "CNS learns stable, accurate, and efficient movements using a simple algorithm," *J. Neurosci.*, vol. 28, no. 44, pp. 11165–11173, 2008.
- [9] K. P. Tee, D. W. Franklin, M. Kawato, T. E. Milner, and E. Burdet, "Concurrent adaptation of force and impedance in the redundant muscle system," *Biol. Cybern.*, vol. 102, no. 1, pp. 31–44, 2010.
- [10] Z. Bien and J. X. Xu, *Iterative Learning Control: Analysis, Design, Integration and Applications*. Norwell, MA: Kluwer, 1998.
- [11] E. Burdet, A. Codourey, and L. Rey, "Experimental evaluation of nonlinear adaptive controllers," *IEEE Control Syst. Mag.*, vol. 18, no. 2, pp. 39–47, Apr. 1998.
- [12] M. Kawato, K. Furukawa, and R. Suzuki, "A hierarchical neural network model for control and learning of voluntary movement," *Biol. Cybern.*, vol. 5, no. 8, pp. 169–185, 1987.
- [13] E. Burdet, K. P. Tee, I. Mareels, T. E. Milner, C. Chew, D. W. Franklin, R. Osu, and M. Kawato, "Stability and motor adaptation in human arm movements," *Biol. Cybern.*, vol. 94, no. 1, pp. 20–32, 2006.
- [14] S. Haddadin, A. Albu-Schäffer, and G. Hirzinger, "Requirements for safe robots: Measurements, analysis & new insights," *Int. J. Robot. Res.*, vol. 28, no. 11, pp. 1507–1527, 2009.
- [15] M. A. Peshkin, J. E. Colgate, W. Wannasupphrasit, C. A. Moore, R. B. Gillespie, and P. Akella, "Cobot architecture," *IEEE Trans. Robot. Autom.*, vol. 17, no. 4, pp. 377–390, Aug. 2001.
- [16] A. Albu-Schäffer, O. Eiberger, M. Grebenstein, S. Haddadin, C. Ott, T. Wimbock, S. Wolf, and G. Hirzinger, "Soft robotics: From torque feedback controlled lightweight robots to intrinsically compliant systems," *IEEE Robot. Autom. Mag.*, vol. 15, no. 3, pp. 20–30, Sep. 2008.
- [17] A. Albu-Schäffer, S. Haddadin, C. Ott, A. Stemmer, T. Wimbock, and G. Hirzinger, "The DLR lightweight robot: Design and control concepts for robots in human environments," *Ind. Robot*, vol. 34, no. 5, pp. 376–385, 2007.
- [18] N. Hogan, "Impedance control: An approach to manipulation—Part I: Theory; Part II: Implementation; Part III: Applications," *Trans. ASME J. Dyn. Syst., Meas. Control*, vol. 107, no. 1, pp. 1–24, 1985.
- [19] C. C. Cheah and D. Wang, "Learning impedance control for robotic manipulators," *IEEE Trans. Robot. Autom.*, vol. 14, no. 3, pp. 452–465, Jun. 1998.
- [20] *Variable Impedance ACTuation systems embodying advanced interaction behaviorS: A project supported by the European Commission under the 7th Framework Programme*. (Jun. 22, 2010). [Online]. Available: [www.viactors.eu](http://www.viactors.eu).
- [21] J. Won and N. Hogan, "Stability properties of human reaching movements," *Exp. Brain Res.*, vol. 107, no. 1, pp. 125–136, 1995.
- [22] R. F. Kirsch, D. Boskov, W. Z. Rymer, R. E. Center, M. H. M. Center, and O. H. Cleveland, "Muscle stiffness during transient and continuous movements of catmuscle: perturbation characteristics and physiological relevance," *IEEE Trans. Biomed. Eng.*, vol. 41, no. 8, pp. 758–770, Aug. 1994.
- [23] H. Gomi and R. Osu, "Task-dependent viscoelasticity of human multijoint arm and its spatial characteristics for interaction with environments," *J. Neurosci.*, vol. 18, no. 21, pp. 8965–8978, 1998.
- [24] T. E. Milner and C. Cloutier, "Compensation for mechanically unstable loading in voluntary wrist movement," *Exp. Brain Res.*, vol. 94, no. 3, pp. 522–532, 1993.
- [25] R. Shadmehr and F. A. Mussa-Ivaldi, "Adaptive representation of dynamics during learning of a motor task," *J. Neurosci.*, vol. 14, no. 5, pp. 3208–3224, 1994.
- [26] A. Jacks, A. Prochazka, and P. S. Trend, "Instability in human forearm movements studied with feed-back-controlled electrical stimulation of muscles," *J. Physiol.*, vol. 402, no. 1, pp. 443–461, 1988.
- [27] D. Rancourt and N. Hogan, "Stability in force-production tasks," *J. Motor Behav.*, vol. 33, no. 2, pp. 193–204, 2001.
- [28] D. W. Franklin, E. Burdet, R. Osu, M. Kawato, and T. E. Milner, "Functional significance of stiffness in adaptation of multijoint arm movements to stable and unstable dynamics," *Exp. Brain Res.*, vol. 151, no. 2, pp. 145–157, 2003.
- [29] D. W. Franklin, R. Osu, E. Burdet, M. Kawato, and T. E. Milner, "Adaptation to stable and unstable dynamics achieved by combined impedance



control and inverse dynamics model," *J. Neurophysiol.*, vol. 90, no. 5, pp. 3270–3282, 2003.

- [30] J. E. Slotine and W. Li, *Applied Nonlinear Control*. Englewood Cliff, NJ: Prentice-Hall, 1991.
- [31] E. J. Perreault, R. F. Kirsch, and P. Crago, "Multijoint dynamics and postural stability of the human arm," *Exp. Brain Res.*, vol. 157, no. 4, pp. 507–517, 2004.
- [32] S. Jagannathan, *Neural Network Control of Nonlinear Discrete-Time Systems*. Boca Raton, FL/New York: CRC/Taylor & Francis, 2006.
- [33] B. Siciliano, L. Sciavicco, L. Villani, and G. Oriolo, *Robotics: Modelling, Planning and Control*. New York: Springer-Verlag, 2008.
- [34] O. Eiberger, S. Haddadin, M. Weis, A. Albu-Schäffer, and G. Hirzinger, "On joint design with intrinsic variable compliance: Derivation of the DLR QA-joint," in *Proc. IEEE Int. Conf. Robot. Autom.*, Anchorage, AK, 2010, pp. 1687–1694.
- [35] L. L. Tien, A. Albu-Schäffer, A. D. Luca, and G. Hirzinger, "Friction observer and compensation for control of robots with joint torque measurement," in *Proc. IEEE/RSJ Int. Conf. Intell. Robots Syst.*, Nice, France, 2008, pp. 3789–3795.
- [36] A. Albu-Schäffer, C. Ott, and G. Hirzinger, "A unified passivity based control framework for position, torque and impedance control of flexible joint robots," *Invited extended version of the Springer Tracts Article, Int. J. Robot. Res.*, vol. 26, no. 1, pp. 23–39, 2007.
- [37] G. Ganesh, M. Haruno, and E. Burdet, "Transitions between reciprocal activation and co-contraction during posture control," *Poster at Neural Control of Movement*, vol. NCM'08, 2008.
- [38] A. Albu-Schäffer, S. Haddadin, C. Ott, A. Stemmer, T. Wimböck, and G. Hirzinger, "The DLR lightweight robot—Lightweight design and soft robotics control concepts for robots in human environments," *Ind. Robot J.*, vol. 34, no. 5, pp. 376–385, 2007.
- [39] A. Tayebi, "Adaptive iterative learning control for robot manipulators," *Automatica*, vol. 40, no. 7, pp. 1195–1203, 2004.



**Sami Haddadin** (M'10) received the Dipl.-Ing. degree in electrical engineering and the M.Sc. degree in computer science from the Technical University of Munich, Munich, Germany, in 2005 and 2009, respectively. He received an Honours degree in technology management from the Technical University of Munich and the Ludwig Maximilian University Munich.

He has been with the German Aerospace Center, Wessling, Germany, since 2005, where he coordinates the human–robot interaction research. His main research interests include physical human–robot interaction, control of actively and passively compliant robots, reactive/reflex planning, and safety and dependability in robotics. Since 2010, he has been lecturing on "Human-Friendly Robotics" at the Technical University of Munich.



**Sven Parusel** received the Dipl.-Inf. degree in computer science from the Kempten University of Applied Sciences, Kempten, Germany, in 2009.

He has been a Research Scientist with the German Aerospace Center, Wessling, Germany, since 2009. His main research interests include physical human–robot interaction and reactive/reflex planning for robots in unstructured environments and in direct interaction with humans.



**Chenguang Yang** (S'07–M'10) received the B.E. degree from the College of Automation, Northwestern Polytechnical University, Xi'an, China, in July 2005 and the Ph.D. degree from the Department of Electrical and Computer Engineering, National University of Singapore, Singapore, in March 2010.

He was a Postdoctoral Research Associate with the Department of Bioengineering, Imperial College London, London, U.K., from October 2009 to December 2010. He is currently a Lecturer in humanoid robotics and intelligent systems with the University of Plymouth, Plymouth, U.K. His current research interests include robotics, control, and human–robot interaction.



**Alin Albu-Schäffer** (M'93) received the M.S. degree in engineering from the Technical University Timisoara, Romania, and the Ph.D. degree in control systems from the Technical University of Munich, Germany, in 1993 and 2002, respectively.

Since 1995, he has been with the Institute of Robotics and Mechatronics, German Aerospace Center, Wessling, Germany. Since 2009, he has been the Head of the Department of Mechatronics Components and Systems. Additionally, since 2007, he has been a Lecturer with the Technical University of Munich, Munich, Germany. His main research interests include the design, modeling, and control of robotic manipulators, especially on compliantly controlled or actuated robots for physical interaction with humans and unknown environments.



**Gowrishankar Ganesh** (M'08) received the B.E. (first-class Hons.) degree from the Delhi College of Engineering, New Delhi, India, in 2002 and the M.E. degree from the National University of Singapore, Singapore, in 2004, both in mechanical engineering, and the Ph.D. degree in bioengineering from Imperial College London, London, U.K., in 2010.

He was an Intern Researcher with the Computational Neuroscience Laboratories, Advanced Telecommunication Research Institute, Kyoto, Japan, between 2004 and 2009, where he is currently a Researcher. Since 2010, he has been a Specialist Researcher with the Advanced ICT group of National Institute of Information and Communications Technology, Tokyo, Japan. His research interests include human motor control, robotics, signal processing, and mechanical design.



**Etienne Burdet** (S'92–M'96) received the M.S. degree in mathematics, the M.S. degree in physics, and the Ph.D. degree in robotics from the Swiss Federal Institute of Technology, Zurich, Switzerland, in 1990, 1991, and 1996, respectively.

He is currently a Reader with Imperial College London, London, U.K. He is doing research at the interface of robotics and bioengineering and his main interest is in human–machine interaction. He has contributions in various fields from human motor control to virtual-reality-based training systems, assistive devices, and robotics for life sciences.